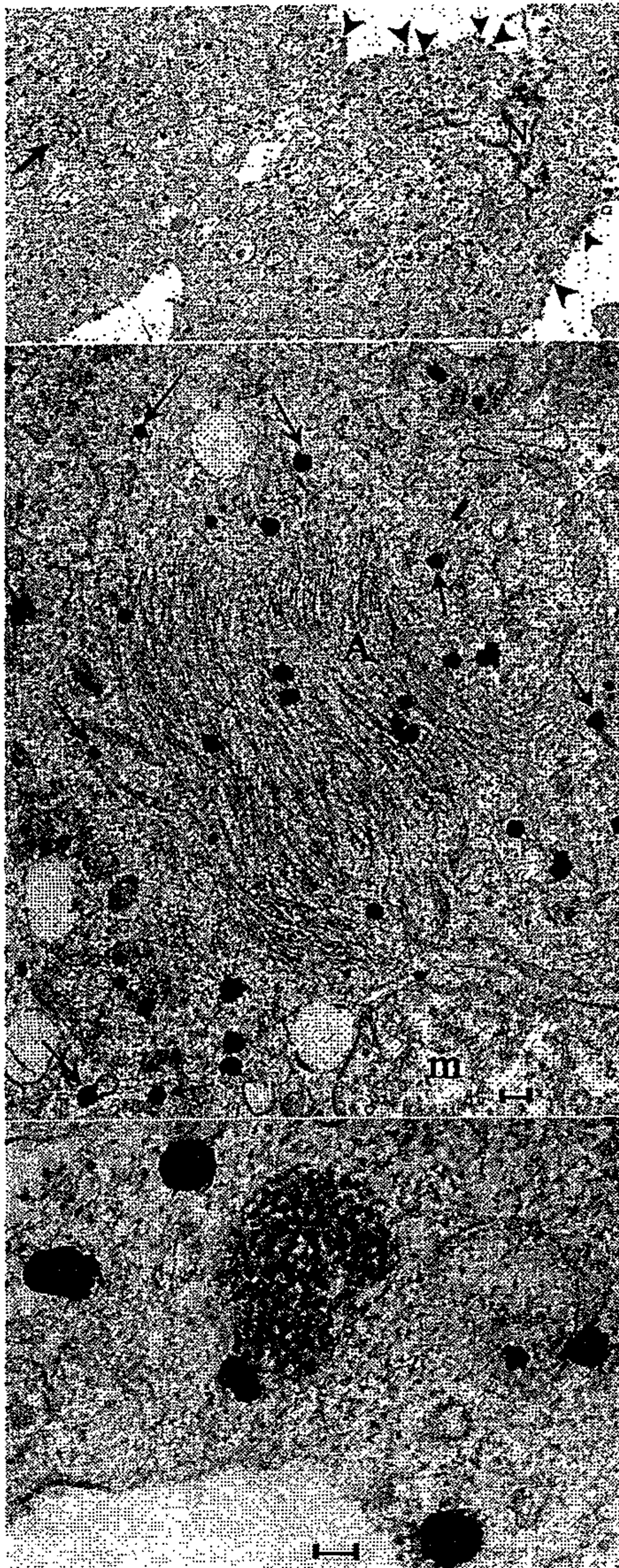

Fig. 3. Ultrasmall immunogold labeling (silver intensified) of PrP and PrP-res in N2a + 22L cells lightly fixed and then permeabilized *in situ* for antigen detection. (*Top*) A typical low-power image where many grains are on the plasma membrane (arrowhead) and dispersed in the cytoplasm. Nuclei (N) and clusters of IAP retroviruses (arrow) are not labeled. (*Middle*) Grains over PrP amyloid fibers in characteristic crisscrossing bundles (A) and also over RER membranes (arrows). Label was not seen over mitochondrial cristae (m) as representatively depicted. (*Bottom*) PrP does not localize over the 25-nm virus-like dense particles but can be associated with the outer RER membrane. (Scale bars: 100 nm.)

abnormal PrP fibrils. A striking feature, most consistent with a viral structure, was the uniform size of the particles in these arrays. This made them easily distinguished from lysosomes with heterogeneous inclusions, as well as other aggregates and dense bodies. The spherical 25-nm particles were variably packed in arrays and, in less compact regions, appeared connected by more lucent stalks. The dense viral spheres had no surrounding vesicular membranes. In compact regions, many of the particles lined up in orthogonal paracrystalline arrays at 90° to each other as in Fig. 1*C* (arrows). Although of similar density as adjacent ribosomes, the 25-nm virus-like particles displayed a more distinct outline and less fuzzy structure. The density of the TSE particles also was comparable with chromatin (a nucleic acid–protein structure), but particle arrays were spatially distant from nuclei, indicating their separate origin (Fig. 1 *A* and *C*). Particle arrays in the membrane-bound bodies overall measured from 0.3 to 1.0 μm across. For internal reference, the IAPs seen in N2a cells are 100 nm in diameter. The C2a subclone of N2a + 22L with a 3- to 4-fold higher PrP-res content also displayed arrays that were morphologically indistinguishable from those in the parental line.

Because cells with virus-like inclusions had normal organelles and were healthy (Fig. 1 *A* and *B*), these virus-like inclusions could not be linked to degenerative processes. Their presence in cells without synapses also demonstrates they did not require elaboration of synaptic structures for their production. In addition, the same dense virus-like particle arrays also were present in GT+FU-CJD cells (Fig. 1*D*). Their presence in a different cell type that was infected by an unrelated TSE agent strain furthered the realization that these particles probably represent the common TSE agent structure. Although individual 25-nm particles outside of the membrane-bound arrays were very difficult to identify with certainty, they were present in some images of both N2a + 22L and GT+FU-CJD cells. Fig. 1*D* shows a few of these individual 25-nm particles that accumulated on or near an RER membrane (arrowhead). This region may represent either a nascent or a disintegrating array that is adjacent to a stack of several pathologic GT cell membranes. Virus-like particle arrays were not found in parallel mock N2a or GT cells.

To further evaluate the potential relationship of these TSE arrays to retroviral expression, PrP-res, and infectivity, we tested several chemical treatments that might alter these components. Phorbol myristate acetate (PMA) can stimulate transcription of viruses, including retroviruses and papovaviruses (19), and also can have other pleomorphic effects, including differentiation. We therefore added PMA to cells and were able to identify conditions that lead to an increase of PrP and PrP-res in infected but not mock N2a cells. Arrays from N2a cells were morphologically unchanged by treatment with PMA, as representatively shown in Fig. 1 *B* and *C*. Fig. 2*A* shows a representative dose–response curve of 22L infected and mock (MK) N2a cells with and without proteinase K (PK) digestion for PrP-res. There is a clear increase in PrP-res at 100 ng/ml for 5 days. No PrP-res is seen in the parallel MK control. Fig. 2*B* shows that the optimized time for this peak response was at 5 days, and the relative loads for each lane are shown by the 54-kDa tubulin internal standard. Fig. 2*C* graphs the quantitative changes in PrP-res in seven independent time course experiments with 75–100 ng/ml PMA (dashed lines). There is a reproducible ≈3.5-fold elevation in PrP-res at 5 days compared with drug-free

infected controls. The solid gray line shows the >5 fold increased PrP-res in the sample used to test whether there was a corresponding increase in titer with this high PrP-res.

We also counted the virus-like particle arrays in N2a + 22L cells that were treated with 100 ng/ml PMA for 5 days and then fixed for electron microscopy. To make sure that any potentially similar particles were not overlooked in mock cells, we included any possible similar virus-like arrays in the count, and hence the percentage of cells with these particles was somewhat overestimated. More than 250 cells each from mock, untreated, and PMA-treated preparations were counted for suspicious virus-like arrays (Fig. 2*D*). Only a single suspect particle could be found in >250 mock cells, and this single photographed inclusion had 7- to 15-nm-wide strings of dense material with no 20- to 35-nm-diameter spherical particles. Thus, no definitive similar virus-like arrays could be found in uninfected cells. As shown in Fig. 2*D*, there was also no significant elevation of particle arrays in the PMA-induced cells with high PrP-res. These molecular evaluations of PrP-res and particle counts were in accord with the spatial separation of virus-like particles and PrP amyloid fibrils, i.e., the two structures were mutually independent.

Ultrastructural studies of control and infected N2a cells also gave the impression of an increase in IAP particles with PMA treatment, but Western blots for IAP gag proteins by using IAP-specific antibodies as described in refs. 16 and 20 failed to confirm any major increase in retroviral proteins (data not shown). The PMA effects on PrP-res also appeared to be cell type and/or agent strain specific because GT+FU-CJD cells did not show any PrP-res increase of similar magnitude with 5 days of PMA at concentrations as high as 200 ng/ml. This high PMA level also did not educe any retroviral particles in GT+FU-CJD cells. Thus, the presence of TSE virus-like arrays in these GT+FU-CJD cells confirmed they were not dependent on, or derived from, retroviruses.

Aliquots of mock, untreated, and PMA-treated N2a cells were analyzed for both PrP-res (Fig. 2*E*) and for infectivity (Fig. 2*F*). In the Western blot of PrP and PrP-res, only the 22L infected cells showed a large increase in PrP-res with PMA treatment, and PMA did not induce either PrP or PrP-res in the uninfected controls (+PK lanes). The particle counts, but not the PrP-res data, predicted there would be no increase in infectivity with PMA stimulation. Thus, aliquots of these cells were inoculated intracerebrally to test whether the titer was increased with the PMA induced PrP-res. Fig. 2*F* shows these bioassays where serial dilutions of the untreated and the PMA-induced N2a + 22L cells were compared (white and gray bars, respectively). There was no significant shortening of the incubation time that would indicate higher infectivity in cells with the higher PrP-res. In fact, the more dilute inocula show that >5-fold increases in PrP-res accumulation yielded slightly longer incubation times. Additionally, the incubation times shown for the PMA-treated and control N2a + 22L cells represent an infectious titer of 1 LD_{50} per ≈3 cells (see *Materials and Methods*). This is a very high level of infection and was comparable with the high titers of GT+FU-CJD cells. Significantly lower levels of infectivity are produced by other TSE cultures, including GT cells infected with 22L scrapie (4, 17). We are aware of no EM images of the 25-nm virus-like particles in other examined TSE cultures, and high levels of infectivity may be required to visualize these particles. Finally, control inoculations with high numbers of mock PMA-treated cells, as expected, yielded no signs of TSE disease in inoculated mice monitored for >300 days (Fig. 2*F*, dotted bar).

Because some abnormal PrP molecules might be in nonamyloid configurations, and normal PrP molecules are probably receptors for the infectious TSE agents (21), we used a third way to resolve whether there was an association of any PrP molecules with the 25-nm particles. Cells were lightly fixed, permeabilized, and then exposed *in situ* to PrP antibodies that detect both the normal and abnormal (N-truncated PrP-res) forms. After secondary ultrasmall gold-labeled detection and silver intensification, many silver grains were present over the plasma membrane (Fig. 3 *Top*, arrowheads) and dispersed through the cytoplasm, but were not over nuclei (N), mitochondria, or IAP clusters (at arrow). This pattern of PrP labeling was entirely consistent with the known residence of normal PrP. Densely packed amyloid fibers also were labeled as shown at A (Fig. 3 *Middle*), indicating good penetration of antibody and detector molecules. This higher magnification also shows that the cytoplasmic PrP label was over RER membranes, as would be expected from the known synthetic routes for a GPI-anchored protein such as PrP. No silver grains were seen over any of the 25-nm virus-like particles, but were sometimes found on the outer RER membrane that encircled the particle arrays (Fig. 3 *Bottom*). The above data contradict the notion that PrP, in any form, is an intrinsic component of the TSE 25-nm virus-like particles.

Discussion

The intracellular 25-nm virus-like dense particles identified here were entirely consistent with a virion shape, size, and viral components as predicted from previous field flow sedimentation, HPLC, and molecular analyses of infectious particles that had been stripped of almost all PrP (16). Unlike host-encoded PrP, they were not detected in uninfected mock controls and, thus, were even more TSE-specific than PrP. They were also not part of the abnormal PrP amyloid, which is believed to be infectious. Furthermore, *in situ* labeling of intact cells, not subject to disruptive and artificial treatments of subcellular fractionation, also showed no association of particle arrays with PrP. Rather, individual 25-nm particles probably associate with PrP in the RER during their assembly, an observation that may explain why a small amount of PrP can remain associated with particles during fractionation. This particle–RER interaction also may initiate the pathological and self-propagating pathological amyloid of TSE disease, as proposed in ref. 21. Because IAP retroviral cores that attach to RER have the same density as the TSE agent (1.28 g/ml) and, therefore, copurify with the TSE agent, residual PrP in more purified infectious 25-nm particle preparations may derive from this source as well.

A recent field flow fractionation study of less pure scrapie brain preparations has reconfirmed the association of comparable ≈25-nm particles with infectivity. This study, however, concluded that these particles were constituted by aggregates of 14–28 PrP molecules, even though there were many other heterogeneous and uncharacterized molecules by silver staining in this peak infectious fraction (22). In contrast, the 25-nm spherical particles from our more purified brain preparations did not bind PrP antibodies (1). Thus, the interpretation of these particles as prions seems tenuous. The failure of PrP antibodies to label the 25-nm particles in cultured cells *in situ*, as well as the PMA-enhanced PrP-res experiments here, also support their nonprion nature. Because images of the particle arrays in our cultures were so virion-like, we researched the largely ignored nonprion literature, and realized (1), as Liberski (12) had emphasized, how common and specific these particles are for TSE-infected brains. Furthermore, as in the above PrP-labeling studies, TSE-infected brain also showed no detectable PrP antibody binding to the 25-nm virus-like particles *in situ* (23). The strong uranyl positive density of these 25-nm particles in brain samples, their size and arrangement into similar orthogonal arrays connected by stalks, the RER membranes surrounding particles arrays, and the specificity of arrays for infected samples all underscored their similarity to the nonprion particles we independently identified here in two different infected cell lines that are free of degenerative morphology.

In the brain, the synaptic location of the TSE virus-like arrays also was consistent with the synaptic concentration of the TSE

NEUROSCIENCE

infectious agent in synaptosomal fractions (24). Additionally, there is one published image of a comparable virus-like array in the perikaryon rather than in postsynaptic boutons (10), further indicating the similarities of the 25-nm particle arrays in brain and cultured cells. Although we did not observe tubular and electron lucent tubular-vesicular/membrane-like components of variable widths in our arrays, as sometimes described in the brain (12), tubular vesicular variants may be due to the elaboration of different components in mature neurons, different stages of particle development, or structures that are not integral to the much denser virus-like particles.

In summation, all of this data provides a clear, consistent, substantive, and logical alternative to the accepted prion hypothesis. The causative TSE agent is most consistent with an exogenous 25-nm virion without intrinsic host PrP. The stimulation of host innate immune responses by these agents, a complex set of molecular reactions that precedes the elaboration of pathologic PrP (9) and one that is not provoked by PrP-res itself (25), also point to a foreign pathogen rather than some unpredictably spontaneous mutation in the host's PrP without cause. The presence of these particles in many different species infected with a wide variety of TSE strains is in accord with Koch's first requirement (1). It is also improbable that an identical virus-like structure would be a contaminant or a secondary coincidental feature of all these different TSE models. Nevertheless, a more detailed molecular analysis of these particles will be required to substantiate their causal nature. Purification of these ≈25-nm particles from productive tissue cultures should be informative if the essential infectivity assays are performed systematically with parallel ultrastructural and molecular analyses. Animal titrations of infectivity are expensive and prolonged. However, sustained and reproducible infection of indicator GT cells by a variety of TSE agents already has shown that they can rapidly authenticate the presence of agent in disrupted samples as well as in living cells (4, 17). GT cells also may be used for testing infectivity of viral nucleic acids as well as PrP conformers. Rapid assays of infectivity in culture should facilitate the isolation of infectious particles from host components, and treatments that modify the production of these particles in culture may resolve further the infectious structure from the pathological disease processes it initiates.

Materials and Methods

Neuroblastoma N2a58 cells infected with the 22L scrapie agent (26) at passage 230 were a gift of N. Nishida (Nagasaki University, Nagasaki, Japan) and were propagated for 50–150 additional passages at Yale, whereas mock N2a58 controls exposed to uninfected brain (4, 17) were passaged in parallel. The C2a subclone of 22L-infected N2a58 cells was also selected for its ≈4-fold higher PrP-res levels; this subclone yielded the same 25-nm particles and, thus, was not further discriminated here. The hypothalamic neuronal GT1.7 cell line that was infected with the FU-CJD agent consistently produced 1–10 LD_{50} per cell by mouse bioassays (4) and repeatedly showed infectivity in a new rapid coculture assay (17). PMA (Sigma, St. Louis, MO) was applied to enhance PrP and PrP-res production in N2a + 22L cells as experimentally determined (see Fig. 2). For infectivity assays, cells were counted, disrupted, diluted, and inoculated intracerebrally into indicator mice as in ref. 4, and titers were calculated from standard incubation time to endpoint dilutions as described in ref. 21 by using 22L-infected brain homogenates inoculated in the same mouse genotype as the standard. Mice were assessed for strain-specific clinical signs and neuropathology by using a panel of standard antibodies (27). For Western blots, whole-cell lysates were analyzed with the M20 PrP antibody (4), and tubulin detection was used to confirm relative lane loads; calibrated chemiluminescent detections were done with an Alpha Innotech imager.

For EM, cells were fixed *in situ* in 2.5% glutaraldehyde in 0.1 M cacodylate buffer, pH 7.4 (CB), for 1 h, harvested by scraping in CB with 1% fish gelatin, pelleted at 500 × *g* for 5 min and then at 3,000 × *g* for 10 min, washed in CB three times for 5 min, and exposed to 1% OsO_4 in CB for 1 h. They then were dehydrated and embedded in Epon 812. For immunolabeling, cells were fixed in 2% paraformaldehyde with 0.25% glutaraldehyde for 1 h, washed with CB, and permeabilized for 30 min at 25°C in CB with 2% normal rabbit serum and 0.2% saponin (Sigma). Cells were then exposed to goat M20 antibody (1:500) against the PrP C terminus (4) for 48 h at 4°C and 2 h at 25°C. After CB washes, cells were incubated at 25°C with 1:500 rabbit anti-goat IgG, washed, exposed to strepavidin ultrasmall gold (1:200; Electron Microscopy Sciences, Hatfield, PA), washed in CB and then H_2O, and enhanced with their silver kit for 15 min. After H_2O washes, cells were osmified and embedded as above. Thin sections were stained with uranyl acetate and lead citrate; photographic negatives were scanned for reproduction.

This work was supported by National Institutes of Health Grant NS 12674 and U.S. Department of Defense Grant DAMD-17-03-1-0360.

1. Manuelidis L (October 16, 2006) *J Cell Biochem*, 10.1002/jcb.21090.
2. Baker CA, Martin D, Manuelidis L (2002) *J Virol* 76:10905–10913.
3. Manuelidis L (2003) *Viral Immunol* 16:123–139.
4. Arjona A, Simarro L, Islinger F, Nishida N, Manuelidis L (2004) *Proc Natl Acad Sci USA* 101:8768–8773.
5. Xi YG, Ingrosso A, Ladogana A, Masullo C, Pocchiari M (1992) *Nature* 356:598–601.
6. Manuelidis L (1998) *Proc Natl Acad Sci USA* 95:2520–2525.
7. Prusiner S (1998) *Proc Natl Acad Sci USA* 95:13363–13383.
8. Manuelidis L, Fritch W (1996) *Virology* 215:46–59.
9. Lu ZH, Baker C, Manuelidis L (2004) *J Cell Biochem* 93:644–652.
10. David-Ferreira J, David-Ferreira K, Gibbs C, Morris J (1968) *Proc Soc Exp Biol Med* 127:313–320.
11. Bignami A, Parry H (1971) *Science* 171:389–390.
12. Liberski P, Jeffrey M (2004) *Folia Neuropathol* 42(Suppl B):96–108.
13. Lampert P, Gadjusek D, Gibbs C (1971) *J Neuropathol Exp Neurol* 30:20–32.
14. Baringer J, Prusiner S (1978) *Ann Neurol* 4:205–211.
15. Sklaviadis T, Dreyer R, Manuelidis L (1992) *Virus Res* 26:241–254.
16. Manuelidis L, Sklaviadis T, Akowitz A, Fritch W (1995) *Proc Natl Acad Sci USA* 92:5124–5128.
17. Nishida N, Katamine S, Manuelidis L (2005) *Science* 310, 493–496.
18. Manuelidis L (1997) *Ann Inst Pasteur (Paris)* 8:311–326.
19. Kim S, Choi E, Woo J, Henson J, Kim H (2004) *Virology* 327:60–69.
20. Akowitz A, Sklaviadis T, Manuelidis L (1994) *Nucleic Acids Res* 22:1101–1107.
21. Manuelidis L, Sklaviadis T, Manuelidis EE (1987) *EMBO J* 6:341–347.
22. Silveira J, Raymond G, Hughson A, Race R, Sim V, Hayes S, Caughey B (2005) *Nature* 437:257–261.
23. Liberski P, Jeffrey M, Goodsir C (1997) *Acta Neuropathol* 93:260–264.
24. Manuelidis L, Manuelidis E (1983) *Banbury Rep (Cold Spring Harbor)* 15:399–412.
25. Baker C, Manuelidis L (2003) *Proc Natl Acad Sci USA* 100:675–679.
26. Nishida N, Harris DA, Vilette D, Laude H, Frobert Y, Grassi J, Casanova D, Milhavet O, Lehmann S (2000) *J Virol* 74:320–325.
27. Manuelidis L, Fritch W, Xi YG (1997) *Science* 277:94–98.

医薬品 研究報告 調査報告書

識別番号・報告回数			報告日	第一報入手日	新医薬品等の区分	機構処理欄
				2007. 1. 12	該当なし	
一般的名称	(製造承認書に記載なし)		研究報告の公表状況	ProMED 20070108-0081, 2007 Jan 8. 情報源:[1]UK Department of Health, Monthly Creutzfeldt-Jakob Disease Statistics, 2007 Jan 8. [2]EUROCJD, 2006 Dec 31.	公表国 英国ほか	
販売名(企業名)	合成血「日赤」(日本赤十字社) 照射合成血「日赤」(日本赤十字社) 合成血-LR「日赤」(日本赤十字社) 照射合成血-LR「日赤」(日本赤十字社)					

研究報告の概要

[1]英国保健省、月次vCJD・CJD統計、2007年1月8日時点
保健省は2007年1月8日、CJD患者数に関する最新情報を公表した。この中にはBSEと関連があると思われるvCJD患者も含まれる。内訳は以下の通り: vCJD患者:vCJD確定例における死亡患者:112名。vCJD可能性例における死亡患者(神経病理学的に未確定):46名。死亡患者総数:158名。vCJD患者-存命中:7名。vCJD確定例または可能性例総数:165名。2006年12月4日の月例統計以来、死亡患者総数には変化なく158名のままである。確定例または可能性例総数は1名増加して165名となった。このデータは英国におけるvCJD流行は減少しつつあるとする見解に一致する。死亡患者数のピークは2000年の28名であり、その後2001年に20名、2002年に17名、2003年に18名、2004年に9名、2005年に5名、2006年に5名と減少している。
[2]EUROCJD
EUROCJDの統計による全世界のCJD患者数の内訳は右表の通りである。

2006年12月時点でのデータ

	患者数累計	生存者	英国滞在6ヵ月以上	輸血による感染疑い
英国	163	7	165	2
フランス	21	2	1	0
アイルランド	4	1	2	0
イタリア	1	0	0	0
米国	3	1	2	0
カナダ	1	0	1	0
サウジアラビア	1	1	0	0
日本	1	0	0	0
オランダ	2	0	0	0
ポルトガル	1	1	0	0
スペイン	1	0	0	0

725

使用上の注意記載状況・その他参考事項等

合成血「日赤」
照射合成血「日赤」
合成血-LR「日赤」
照射合成血-LR「日赤」

血液を介するウイルス、細菌、原虫等の感染
vCJD等の伝播のリスク

報告企業の意見

英国保健省発表の統計によると、2007年1月8日時点で、vCJD確定例または可能性例総数は165名で、死亡患者総数には変化なく158名のままであり、英国におけるvCJD流行は減少しつつあるとする見解に一致するとの報告である。

今後の対応

日本赤十字社は、vCJDの血液を介する感染防止の目的から、献血時に過去の海外渡航歴(旅行及び居住)を確認し、欧州36ヶ国に一定期間滞在したドナーを無期限に献血延期としている。また、英国滞在歴を有するvCJD患者が国内で発生したことから、平成17年6月1日より英国滞在歴1日以上の方からの献血を制限している。さらに、さらに、血液製剤の保存前白血球除去を導入し、平成19年1月16日には全ての輸血用血液への保存前白血球除去の導入が完了した。今後もCJD等プリオン病に関する新たな知見及び情報の収集に努める。